RSC Advances

ROYAL SOCIETY OF CHEMISTRY

www.rsc.org/advances

Cite this: DOI: 10.1039/c0xx00000x

www.rsc.org/xxxxxx

ARTICLE TYPE

Novel Cu_2S quantum dots coupled flower-like BiOBr for efficient photocatalytic hydrogen production under visible light

Baoxiang Wang[2], Weijia An[1], Li Liu[1], Wei Chen[2], Yinghua Liang[1*], Wenquan Cui[1*]

Received (in XXX, XXX) Xth XXXXXXXXX 20XX, Accepted Xth XXXXXXXXX 20XX
DOI: 10.1039/b000000x

Cu_2S quantum dots (QDs) coupled three-dimensional (3D) flower-like hierarchical BiOBr (QDs-Cu_2S/BiOBr) were prepared via a simple precipitation method. The Cu_2S QDs, with an average diameters of 10 nm, were uniformly attached on the surface of BiOBr with an intimately contact interface and evidenced by characterization of the structure and composition of the composite. The QDs-Cu_2S/BiOBr composite exhibited enhanced water splitting for hydrogen evolution, and 717 μmol/g of H_2 was produced with 3 wt% QDs-Cu_2S/BiOBr containing 1 wt% Pt, which was 3.1 times higher than that of Cu_2S nanoparticles. The enhancement of hydrogen evolution was attributed to the synergic effect between BiOBr and Cu_2S QDs, where the hybridization could effectively accelerate the separation of the photogenerated charge carriers.

1. Introduction

Photocatalytic hydrogen production via water splitting over semiconductors under solar irradiation has been regarded as an urgent topic due to its potential applications in renewable energy and environmental cleaning [1-3]. The semiconductor Cu_2S exhibits great potential in hydrogen production due to the desired band-gap width and suitable band structure [4]. Furthermore, the Cu_2S possessed abundant pairs of available electrons states, which was beneficial to the photocatalytic activity [5]. Moreover, semiconductor quantum dots have attracted considerable attention in photocatalytic hydrogen production [6,7]. The higher photon conversion efficiencies and the larger specific surface area were all contribute to the hydrogen production [8,9]. However, the high recombination rates of photogenerated electron-hole pairs and the reunite of Cu_2S QDs significantly decreased the photocatalytic efficiency and limited its practical application [10]. Hence, great efforts should dedicate to reducing the recombination of the photo-induced electron-holes and further to improve the photocatalytic performance.

It is generally accepted that loading Pt could greatly improve the hydrogen evolution efficiency of photocatalysts from water splitting in the presence of sacrificial reagents [11], where the Pt act as electron acceptor and hydrogen production center [12]. Tran's group [13] has reported Cu_2O-rGO composites with Pt loading could enhance hydrogen generation, meanwhile, they pointed that the deactivation of Pt-decorated Cu_2O nanoparticles was due to the less efficient interfacial interaction between Pt and Cu_2O nanoparticles, and the rGO in this system provides enhancing interfaces and facilitates the migration of the electron-hole pairs. Meanwhile, our group previous report confirmed that depositing Cu_2S nanoparticles on the surface of the unique layered structure $K_4Nb_6O_{17}$, the coupled energy levels could effectively accelerated the separation of the photogenerated charges, thus to enhance the hydrogen evolution [14]. This above results gave us the inspiration to introduce a semiconductor which could provide large contact interface and to separate the photogenerated charge carriers.

Recently, the three-dimensional (3D) flower-like hierarchical BiOBr has attracted much attention due to the special flower-like structure which could provide the larger specific surface area and the excellent photocatalytic performance [15-17]. Fabrication of heterostructured materials containing BiOBr could further improve the charge separation through the synergetic effect between the coupled semiconductors caused by their suitable band levels, such as C_3N_4 [18], $ZnFe_2O_4$ [19], AgBr [20], Ag@AgX [21] etc. Actually, the BiOBr possessed the well-aligned overlapping band-structures with Cu_2S which seems to effectively separate the photogenerated carriers. Furthermore, the unique nanosheet building blocks of BiOBr microsphere could act as clapboards to separate Cu_2S QDs and provide more reactive sites to the photocatalysts [22], which could obtain a higher specific surface area and more reactive sites to the photocatalysts, thus was favorable for its photocatalytic activity.

All these results motivate us to design the novel QDs-Cu_2S/BiOBr composites to enhance the hydrogen production under visible light irradiation, where the BiOBr not only act as excellent supporting materials to improve the dispersion of the Cu_2S QDs, but greatly accelerate the migration of the photogenerated charges of Cu_2S, which was favorable for its hydrogen production.

2. Experimental

2.1. Synthesis of photocatalysts

The flower-like BiOBr microsphere was synthesized through the reported by our group previously [23]. All of the reagents used for synthesis were commercially available and used without further purification. The Cu_2S QDs decorated BiOBr samples were prepared via a simple precipitation method. In a typical procedure, measured amounts of cetyl trimethyl ammonium bromide (CTAB) and ethylene diamine tetra acetic acid (EDTA) added into 20 mL deionized water under stirring for 30 min to obtain a uniform suspension. Then, 0.5 g BiOBr added into the solution and stirred until the BiOBr was homogeneously dispersed in the solution. Then, 10 mL $Cu(Ac)_2$ aqueous solution (0.3 mM) was subsequently dropwised into the solution and stirred for 30 min, the solution color gradually changed to blue. After that, 10 ml Na_2S (0.15 mM) solution was added dropwise. Upon addition, the solution immediately changed to rubricans, indicating the formation of Cu_2S nanoparticles. After 30 min, 20 mL of AA (0.3 $mol \cdot L^{-1}$) solution was added dropwise to the solution. The obtained samples were rinsed several times with ethanol, and then dried under vacuum. For comparison, pure Cu_2S particles were synthesized using the same procedures without the addition of BiOBr.

2.2. Characterization of the photocatalysts

The crystal phases of the catalysts were evaluated by powder X-ray diffraction (XRD, D/MAX2500PC, Cu Kα, 40 kV, 100 mA) scanning over the two-theta range of 5-80°. The morphologies of the catalysts were examined by scanning electron microscopy (SEM, Hitachi, s-4800) and transmission electron microscopy (TEM, JEM-2010, 200 kv). UV-vis diffuse reflectance spectra were obtained by using a Puxi, UV1901 spectrometer with $BaSO_4$ as a reference and the chemical compositions of the catalysts were studied by energy dispersive X-ray spectroscopy (EDS, Thermo Noran 7). Surface areas of the samples were determined using a Brunauer-Emmett-Teller (BET) estimation based on the N_2 sorption isotherms collected using a Quantachrome Nova 4200e automatic analyzer (USA). To study the recombination of photo induced charge carriers, photoluminescence (PL, Hitachi F-7000, 250 nm) spectra were collected. The photoelectrochemical measurements were measured on an electrochemical system (CHI-660B, China), using a conventional three-electrode cell. BiOBr and QDs-Cu_2S/BiOBr electrodes served as the working electrode. The counter and the reference electrodes were a platinum wire and a saturated calomel electrode (SCE), respectively, and 0.1 M Na_2SO_4 was used as electrolyte solution. Potentials are given with reference to the SCE. The photoelectric responses of the photocatalysts as light on and off were measured at 0.0 V. Electrochemical impedance spectra (EIS) were measured at 0.0 V. A sinusoidal ac perturbation of 5 mV was applied to the electrode over the frequency range of 0.05-105 Hz.

2.3. Photocatalytic activity

Photocatalytic hydrogen production of the photocatalyst samples were performed in a top irradiation system. In a typical experiment, 0.3 g of photocatalyst powder was dispersed in a 100 mL of aqueous solution of 0.1 M Na_2S and 0.5 M Na_2SO_3. A certain amount of $H_2PtCl \cdot 6H_2O$ aqueous solution was dripped into the system to load 1 wt% Pt onto the surface of the photocatalysts by a photochemical reduction deposition method. The temperature of the reaction was controlled at 25±2 °C and the light source used was a 300 W xenon lamp equipped with a filter to remove light with wavelengths below 400 nm. Before the photocatalytic experiments, the whole system was flushed with Ar gas for 30 min to remove dissolved oxygen and ensured the reaction system under anaerobic conditions. The produced hydrogen was detected using an online gas chromatography (SHIMADZUGC-2014C, molecular sieve 5 A column, TCD detector, Ar carrier).

3. Result and discussion

The XRD patterns of the as-prepared composites were shown in Fig. 1(a). For the spectra of pure BiOBr, characteristic diffraction peaks were detected at 2θ angles of 8.11°, 25.2°, 31.7°, 32.2°, 46.2°, and 57.1°, attributed to the (001), (101), (102), (110), (200), and (212) crystal planes, respectively, as indexed by BiOBr (JCPDS 09-0393). And the BiOBr possessed a high degree of crystallinity based on the intensity of the diffraction peaks obtained. The XRD patterns of the as-prepared QDs-Cu_2S/BiOBr composites were quite similar to the BiOBr, indicating that the introduction of the Cu_2S QDs did not bring any influence on the crystal structure and the lattice structure of BiOBr [24]. The intensity of the (001) crystal planes of BiOBr decreased with increasing of Cu_2S QDs content, this phenomenon was attributed to the Cu_2S QDs gradually covered the surface of BiOBr. However, no typical peaks attributed to Cu_2S were detected, due to the small particle size and quantity of Cu_2S QDs dopant as well as their high dispersion. The existence of Cu_2S QDs was further identified by the SEM, EDS and XPS. Fig. 1(b) shows the XRD pattern for the pure Cu_2S sample. The major diffraction peaks could be detected and well assigned to Cu_2S (JCPDS 65-3288).

The morphology and microstructure of the prepared samples were revealed by SEM, TEM and HRTEM. As shown in Fig. 2(a), the as-prepared three dimensional BiOBr hierarchical microspheres (with diameters of 3-5 μm) were constructed by numerous two dimensional (2D) interlaced nanosheets. These interlaced nanosheets were aligned from the sphere center to the surface to form hierarchical microspheres with an open porous structure. The 3 wt% QDs-Cu_2S/BiOBr composite exhibited the similar morphology with the pure BiOBr (as seen in Fig. 2b), the Cu_2S QDs were homogeneously coated on the surface of the BiOBr, the nano-sheets acted as clapboards to separate Cu_2S QDs, indicating the BiOBr was the excellent supporting materials to improve the dispersion of the Cu_2S QDs, caused a higher surface-to-volume ratio and more reactive sites to the photocatalysts, which was favorable for its photocatalytic hydrogen evolution activity. The EDS patterns of the 3 wt% QDs-Cu_2S/BiOBr composite was in the inset of Fig. 2(b), Bi, Br and O peaks coming from BiOBr, Cu and S diffraction peaks corresponding to

Cu_2S were also observed, confirming that the sample was composed of BiOBr and Cu_2S. Besides, the associated EDS elemental maps were obtained to evaluate the chemical uniformity within individual particles, which clearly confirmed that the Cu_2S QDs were uniformly distributed on the surface of the BiOBr microsphere (as seen in Fig. 3). To further investigate the morphology and detail structural information of the QDs-Cu_2S/BiOBr catalyst, TEM and HRTEM were performed on the 3 wt% QDs-Cu_2S/BiOBr composite. Fig. 2(c) displayed the TEM image of individual microsphere with a magical circle, in accordance with the above SEM images. From the enlarged fraction of the microsphere edge could observed the Cu_2S QDs, with a uniformly shape and size about 10 nm, were observed homogeneously coat on the surface of the single layer of BiOBr with a closely contacted interface, which plays an important role for separation of the photogenerated charges. Furthermore, the various lattices spacing present were observed from the HRTEM image (as seen in Fig. 2d), demonstrated the lattice fringes of BiOBr and Cu_2S could be observed, and the interplanar spacings were measured to be 0.20 and 0.28 nm, coupled with the XRD analysis, which could be assigned to the (220) plane of Cu_2S and the (102) plane of BiOBr, respectively, indicating the intimately contact between BiOBr and Cu_2S.

XPS spectra for the 3 wt% QDs-Cu_2S/BiOBr composites were presented to determine the oxidation state and elemental composition for each member of the composites. From the Bi 4f XPS spectra shown in Fig. 4(a), two strong peaks center at 159.15 eV and 164.5 eV are observed, attribute to Bi 4f7/2 and Bi 4f5/2, respectively, implied that Bi was mainly present in its tri-valent chemical state [20]. The high resolution spectrum of Cu 2p (Fig. 4b) reveals that the two peaks are 932.1 eV and 952.1 eV, attribute to Cu 2p3/2 and Cu 2p1/2, respectively, which are consistent with those observed in Cu_2S [25,26]. The resulting S 2p spectrum (Fig. 4c) shows one peak at a binding energy of 161.8 eV, in agreement with the accepted binding energy value for S^{2-} in Cu_2S [27,28]. From the Fig. 4(d), the peak for O 1s appeared at 531.1 eV, and was resolved into two peaks at 530.4 eV and 531.7 eV, which were assigned to the lattice oxygen and hydroxyl oxygen, respectively [21]. In addition, the XPS spectra of element Cu and S after the photocatalytic hydrogen reaction have been added (as seen in Fig. 4(b, c)), there was no evident shift of the peak pattern besides the intensity was a little decreased, which verified the stability of the photocatalysts. Therefore, combining SEM, EDS and XPS investigations, the results confirmed that there were both BiOBr and Cu_2S species in the composites.

The optical properties of the as-prepared samples showed in Fig. 5. The prepared BiOBr exhibited absorption up to 450 nm and all the QDs-Cu_2S/BiOBr samples exhibited red shift when compared with BiOBr, due to the photosensitizing effect of the incorporated Cu_2S QDs [29]. It owing to the band gap of Cu_2S being 1.2 eV, which could absorb a majority of visible light. In addition, it is noteworthy that there was an obvious positive correlation between the Cu_2S QDs content and the absorption intensity. These results indicated that the QDs-Cu_2S/BiOBr composites could motivate more photogenerated charge carriers which were beneficial for the hydrogen production.

Molecular fluorescence spectroscopy was an effective measure to study the recombination of the photogenerated electron-hole pairs [30]. As showed in Fig. 6, a strong emission peak was observed at 465 nm, due to the recombination of the electron hole pairs of BiOBr. However, the intensity was significantly decreased upon introduction of Cu_2S QDs, indicating that the recombination of the photo-excited electrons and holes was greatly restrained. Such a dramatic decrease of PL intensity meant highly efficient electron transfer in the QDs-Cu_2S/BiOBr composites, which was favorable for its photocatalytic activity.

Photocurrent could directly display the mobility capability of the photogenerated electrons, and the higher peak intensity represented the higher separation of the photogenerated carriers [31], which has a positive correlation with the photocatalytic activity of the photocatalyst directly [32]. The photo-responses of BiOBr and QDs-Cu_2S/BiOBr samples were performed under several on/off sunlight irradiation cycles shown in Fig. 7(a). It was noted that the pure BiOBr showed almost no photocurrent response. On the contrary, the 3 wt% QDs-Cu_2S/BiOBr composites exhibited significantly improvement under visible light irradiation, indicated that the higher transfer of the photogenerated carriers in the 3 wt% QDs-Cu_2S/BiOBr composites.

Furthermore, electrochemical impedance spectroscopy (EIS) was also used to investigate the interface charge separation efficiency between the photogenerated electrons and holes [33]. The smaller arc radius of an EIS Nyquist plot, the higher efficiency of interfacial charge transfer and the more effective separation of photogenerated electron-hole pairs [34]. It was clearly observed that the diameter of the semicircle became shorter upon introduced of Cu_2S QDs (Fig. 7b), meant that the 3 wt% QDs-Cu_2S/BiOBr composites possessed faster interfacial charge transfer efficiencies and the effective separation of photogenerated charge carriers. The results of the PL, photocurrent and EIS measurements were consistent and indicated that couple the Cu_2S QDs and BiOBr could effective to facilitate the separation of photogenerated electron-hole pairs, and then to improve the hydrogen production.

Photocatalytic hydrogen production activities of the as-prepared composites loading with 1 wt% Pt were evaluated under visible light irradiation for 3 h in aqueous solution with 0.1 M Na_2S, 0.5 M Na_2SO_3 as sacrificial agents. As seen in Fig. 8(a), no hydrogen evolution was observed in the presence of BiOBr, and the pristine Cu_2S nanoparticles without Pt exhibited a relatively low H_2

production (94.31μmol/g) due to the high recombination rate of the photogenerated charges at the Cu_2S QDs surface [35]. The nanoparticles Cu_2S with 1 wt% Pt exhibited higher hydrogen evolution (241.2μmol/g) meant the Pt was a great electrocatalyst for H_2 production [36]. Interestingly, the 3 wt% QDs-Cu_2S/BiOBr composites with 1 wt% Pt loading could substantially improve the hydrogen evolution (717 μmol/g), which was 3.1 times higher than pure Cu_2S nanoparticles, indicating the BiOBr played an important role in enhancing the hydrogen evolution in the system. The nanosheet building blocks of BiOBr microsphere could effective to separate Cu_2S QDs and the synergistic effect between BiOBr and Cu_2S QDs could effectively accelerate the charge separation at the intimately contact interface. Furthermore, a mixture of pristine Cu_2S nanoparticles and BiOBr (with a weight ratio was 3/100) was also performed, the hydrogen production was much lower than achieved for 3 wt% QDs-Cu_2S/BiOBr composites, indicating that the mixing of Cu_2S nanoparticles and BiOBr could not result in an efficient photogenerated charge transport. Meanwhile, a significant impact of Cu_2S QDs content was found in Fig. 8(b), where clearly observed that the hydrogen evolution increased with increasing of Cu_2S QDs contents, and the highest activity obtained for the 3 wt% QDs-Cu_2S/BiOBr composites. However, further increasing the content of Cu_2S would lead to a reduction of the photocatalytic activity, due to the overloading of the Cu_2S QDs tended to agglomerate to some extent, which could reduce the specific surface area and the density of active sites for hydrogen production [37]. Additionally, at higher loadings, the Cu_2S may act as recombination centers rather than separation of the photogenerated charges [38].

To evaluate the stability of the QDs-Cu_2S/BiOBr composites, repeated experiments were carried out on the H_2 production activity of the 3 wt% QDs-Cu_2S/BiOBr composites. As seen in Fig. 9, the high photocatalytic performance of 3 wt% QDs-Cu_2S/BiOBr was effectively maintained after five cyclic experiments. A slight decrease of H_2 evolution was observed after irradiation for 15 h, implied reliable stability under the experimental periods. The slight decrease of H_2 evolution was thought to be the loss of the catalyst during the photocatalytic trials as suggested by other researchers [39]. XRD analysis of the catalyst before and after the cycling experiment (Fig. 9b) also illustrated the relative stability of the photocatalyst, since the crystal structure observed did not change significantly. All these results confirming that the QDs-Cu_2S/BiOBr composites exhibit great potential in the practical application.

It is generally accepted that the photocatalytic activity was mainly governed by the photogenerated charge separation efficiency. According to the data reported in the literature [14,30], the valance band of BiOBr and Cu_2S were 3.18 and 1.14 eV, and their homologous conduction band were 0.30 and -0.06 eV vs NHE, respectively, confirming that BiOBr and Cu_2S possessed a well-coupled band structure, which was favorable for the separation of photogenerated carriers. As seen in Fig. 10, the electric field at the surface of the composite could to push the electrons from the conduction band of Cu_2S to conduction band of BiOBr and then transfer to Pt to produce H_2 [10,12,19]. Meanwhile, the photogenerated holes were effectively collected in the VB of Cu_2S, and could scavenged by the mixing solution of Na_2S and Na_2SO_3[25,40]. As a result, the photogenerated electron-hole pairs were thought to be effectively separated, in accordance with the results of the PL, photocurrent and EIS measurements. Furthermore, the specific surface area was enlarge when loading the Cu_2S QDs onto the BiOBr (the specific surface area of BiOBr and 3 wt% QDs-Cu_2S/BiOBr was 6.11 and 11.82 m^2/g, respectively), since the BiOBr act as excellent supporting materials, which could reduce the agglomeration of the Cu_2S QDs and enhance the adsorption of H_2O molecules. Based on these considerations, the QDs-Cu_2S/BiOBr composites exhibited enhancement photocatalytic activity.

4. Conclusions

In summary, we have successfully developed a simple precipitation method to couple Cu_2S QDs and flower-like hierarchical BiOBr. The 3 wt% QDs-Cu_2S/BiOBr composites containing 1 wt% Pt showed a highest hydrogen evolution. The enhancement hydrogen evolution was thought to be the synergistic effect between BiOBr and Cu_2S QDs, where the well-matched overlapping band-structures and the intimate contact interface were beneficial for the separation of the photogenerated carriers. Furthermore, it should be noted that the 3D hierarchical BiOBr improved the dispersion and inhibited the agglomeration of the Cu_2S QDs as excellent supporting materials. The finding highlights the validity of couple Cu_2S and 3D hierarchical semiconductor as effective photocatalysts.

Acknowledgements

This work was supported by the National Natural Science Foundation of China (grant Nos. 51172063, 51202056, 51372068), Hebei Natural Science Funds for Distinguished Young Scholar (grant No. B2014209304), Hebei Natural Science Funds for the Joint Research of Iron and Steel (grant No. B2014209314), Hebei Provincial Foundation for Returned Scholars. Baoxiang Wang and Weijia An contributed equally to this work.

Notes and references

[1] *College of Chemical Engineering, Hebei United University, Tangshan 063009, PR China*

[2] *College of Metallurgy and Energy, Hebei United University, Tangshan 063009, PR China*

Tel.: +86 315 2592169; E-mail: wkcui@163.com, liangyh@heuu.edu.cn

1. Wang C L, Astruc D. *Chem. Soc. Rev*, 2014, 43, 7188-7216.
2. Cho I S, Chen Z B, Forman A J *et al. Nano Lett*. 2011, 11, 4978-4984.
3. Tong H, Ouyang S X, Bi Y P *et al. Adv. Mater*. 2012, 24, 229-251.
4. Bryks W, Wette M, Velez N *et al. J. Am. Chem. Soc*. 2014, 136, 6175-6178.

5. Plante I J L, Teitelboim A, Pinkas I *et al*. *J. Phys. Chem. Lett*. 2014, 5, 590-596.
6. Apte S K, Garaje S N, Naik S D *et al*. *Nanoscale*. 2014, 6, 908-915.
7. Su Y J, Lu X N, Xie M M *et al*. *Nanoscale*. 2013, 5, 8889-8893.
8. Xiao F X, Miao J W, Liu B *et al*. *J. Am. Chem. Soc*. 2014, 136, 1559-1569.
9. Michalet X, Pinaud F F, Bentolila L A *et al*. *Science*. 2005, 28, 538-544.
10. Jiang Y, Zhang X, Ge Q Q *et al*. *Nano Lett*. 2014, 14, 365-372.
11. Li Q, Guo BD, Yu J G *et al*. *J. Am. Chem. Soc*. 2011, 133, 10878-10884.
12. Chowdhury P, Malekshoar G, Ray M B *et al*. *Ind. Eng. Chem. Res*. 2013, 52, 5023-5029.
13. Tran P D , Batabyal S K, Pramana S S *et al*. *Nanoscale*. 2014, 4, 3875-3878.
14. Liang Y H, Shao M Y, L Liu *et al*. *Catal. Commun*. 2014, 46, 128-132.
15. Cheng H F, Huang B B, Wang Z Y *et al*. *Chem Eur J*. 2011, 17, 8039-8043.
16. Zhang H J, Yang Y X , Zhou Z *et al*. *J. Phys. Chem. C*. 2014, 118, 14662-14669.
17. Ye L Q, Su Y R, Jin X L, *et al*. *Appl. Surf. Sci*. 2014, 311, 858-863.
18. Fu J, Tian Y L, Chang B B *et al*. *J Mater Chem*. 2014, 22, 21159-21166.
19. Kong L, Jiang Z, Xiao T C *et al*. *Chem. Commun*. 2011, 47, 5512-5514.
20. Kong L, Jiang Z, Lai H H *et al*. *J. Catal*. 2012, 293, 116-125.
21. Ye L Q, Liu J Y, Gong C Q *et al*. *ACS Catal*. 2012, 2, 1677-1683.
22. Cheng H F, Huang B B, Wang P *et al*. *Chem Commun*. 2011, 47, 7054-7056.
23. Cui W Q, An W J, Liu L *et al*. *J. Hazard. Mater*. 2014, 280, 417-427.
24. Hou J G, Wang Z, Jiao S Q *et al*. *CrystEngComm*. 2012, 14, 5923-5928.
25. Schneider S, Ireland J R, Hersam M C *et al*. *Chem. Mater*. 2007, 19, 2780-2785.
26. Lee H J, Yoon S W, Kim E J *et al*. *Nano Lett*. 2007, 7, 778-784.
27. Li X M, Shen H B, Niu J Z *et al*. *J. Am. Chem. Soc*. 2010, 132, 12778-12779.
28. Zhang X, Guo Y G, Liu W M. *Mater Lett*. 2009, 63, 982-984.
29. Chang J Y, Su L F, Li C H *et al*. *Chem. Commun*. 2012, 48, 4848-4850.
30. Hou J G, Yang C, Cheng H J *et al*. *Phys. Chem. Chem. Phys*. 2013, 15, 15660-15668.
31. Liu Y F, Lv Y H, Zhu Y Y *et al*. *Appl. Catal. B: Environ*. 2014, 147, 851-857.
32. McShane C M, Choi K S. *J. Am. Chem. Soc*. 2009, 131, 2561-2569.
33. Lv Y H, Liu Y F, Zhu Y Y *et al*. *J. Mater. Chem. A*. 2014, 2, 1174-1182.
34. Leng W H, Zhang Z, Zhang J Q *et al*. *J. Phys. Chem. B*. 2005, 109, 15008-15023.
35. Maji S K, Dutta A K, Bhadu G R *et al*. *J. Mater. Chem. B*. 2013, 1, 4127-4134.
36. Chai B, Peng T Y, Zeng P *et al*. *J. Mater. Chem*. 2011, 21, 14587-14593.
37. Liu X L, Zhou M J, Yao G X *et al*. *RSC Adv*. 2014, 4, 18264-18269.
38. Wang D J, Guo L, Zhen Y Z *et al*. *J. Mater. Chem. A*. 2014, 2, 11716-11727.
39. Li Y Y, Ding Y. *J. Phys. Chem. C*. 2010, 114, 3175-3179.
40. Zhang Y Y, Wang Y H, Jin J *et al*. *ACS Appl. Mater. Interfaces*. 2013, 5, 10317-10324.

Figure captions

Fig.1 (a) XRD patterns of the as-prepared BiOBr and QDs-Cu_2S/BiOBr samples; (b) XRD pattern of Cu_2S

Fig. 2 SEM images of prepared photocatalysts (a) BiOBr; (b) 3 wt% QDs-Cu_2S/BiOBr, inset: the EDS spectrum of 3 wt% QDs-Cu_2S/BiOBr; (c, d) TEM and HRTEM micrographs of 3 wt% QDs-Cu_2S/BiOBr composite

Fig. 3 SEM image of 3 wt% QDs-Cu_2S/BiOBr, and Br, Bi, O, Cu and S elemental maps of different particles in 3 wt% QDs-Cu_2S/BiOBr

Fig. 4 High-resolution XPS spectra of the 3 wt% QDs-Cu_2S/BiOBr sample, (a) Bi 4f, (b) Cu 2p (black line: before photocatalysis; red line: after photocatalysis), (c) S 2p (black line: before photocatalysis; red line: after photocatalysis), (d) O 1s

Fig. 5 UV-vis diffuses reflectance spectra of the BiOBr and various QDs-Cu_2S/BiOBr.

Fig. 6 Photoluminescence (PL) spectra of BiOBr and QDs-Cu_2S/BiOBr samples (λex=250 nm)

Fig. 7 (a) Transient photocurrent response for the pure BiOBr and 3 wt% QDs-Cu_2S/BiOBr samples; (b) Electrochemical impedance spectroscopy for the pure BiOBr and 3 wt% QDs-Cu_2S/BiOBr samples

Fig. 8 (a) Comparison of photocatalytic H_2 production activities of various composites; (b) hydrogen production activity of various Cu_2S QDs loadings photocatalysts

Fig. 9 (a) Cycling runs for the H_2 production over 3 wt% QDs-Cu_2S/BiOBr composite; (b) XRD patterns for the fresh and recycled 3 wt% QDs-Cu_2S/BiOBr

Fig. 10 The proposed photocatalytic H_2 production mechanism for QDs-Cu_2S/BiOBr composite

Fig. 1

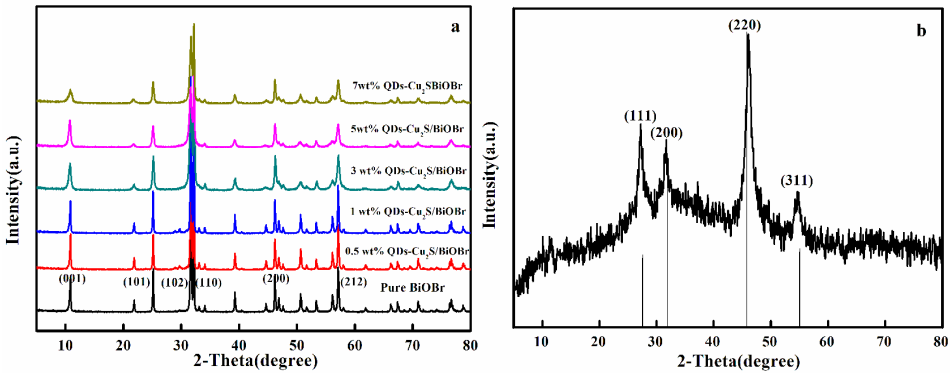

Fig. 2

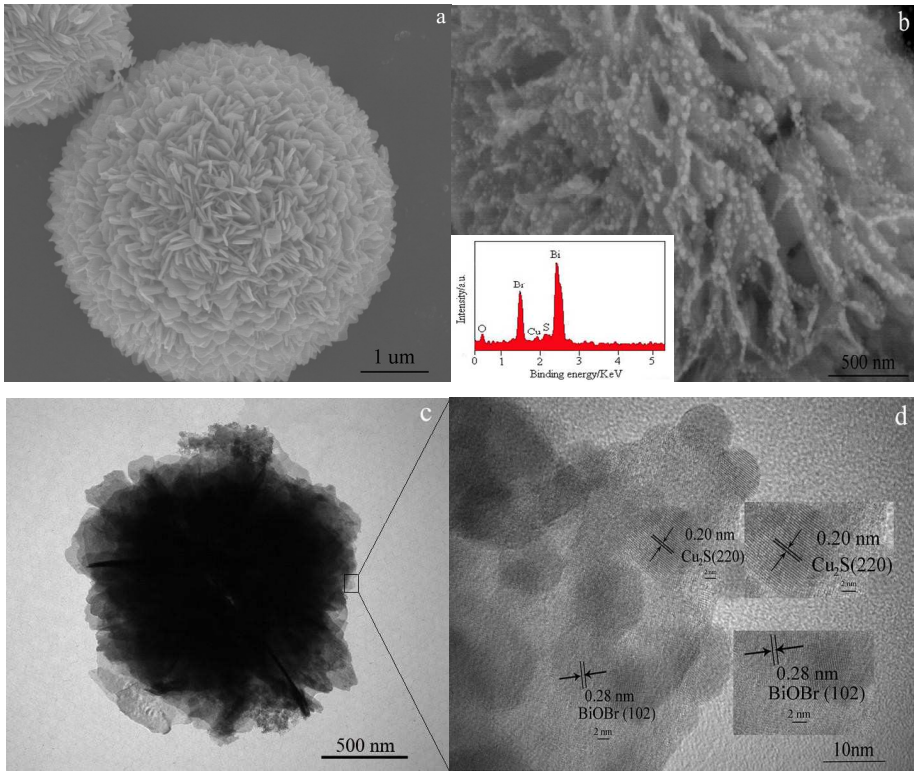

Fig. 3

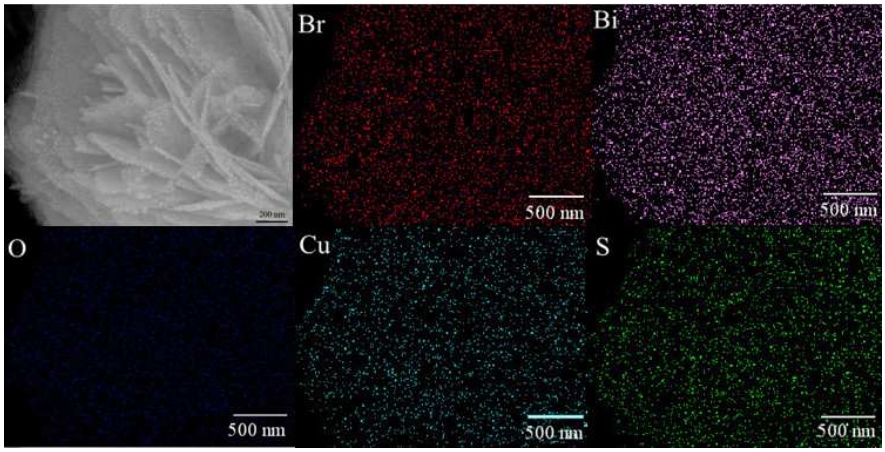

Fig. 4

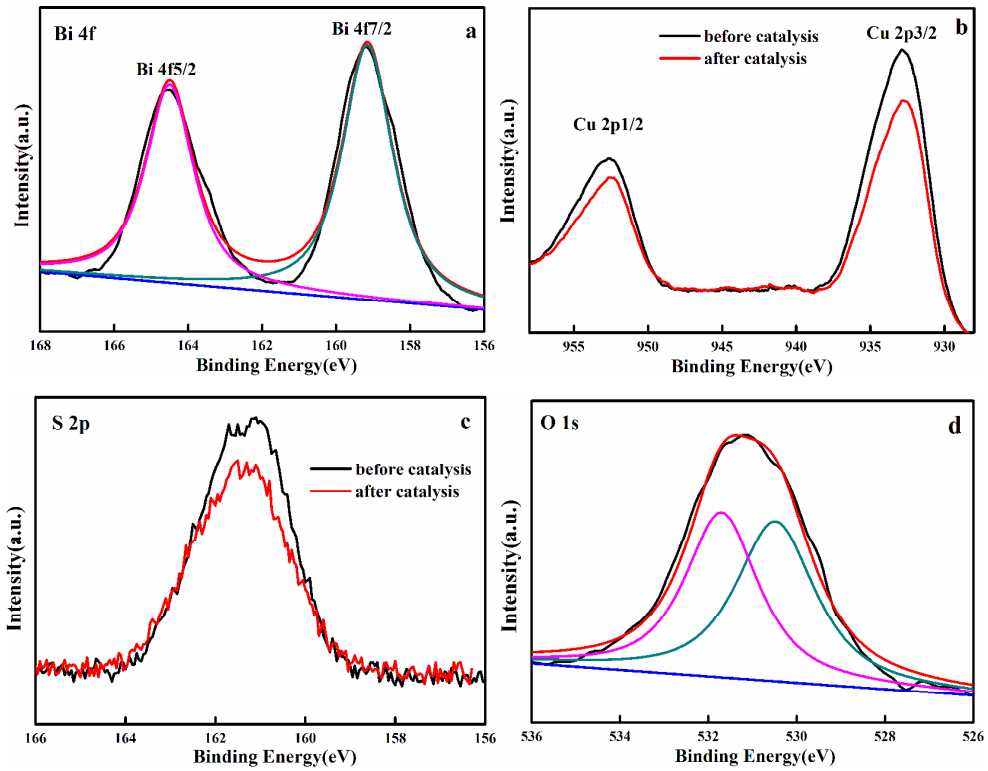

Fig. 5

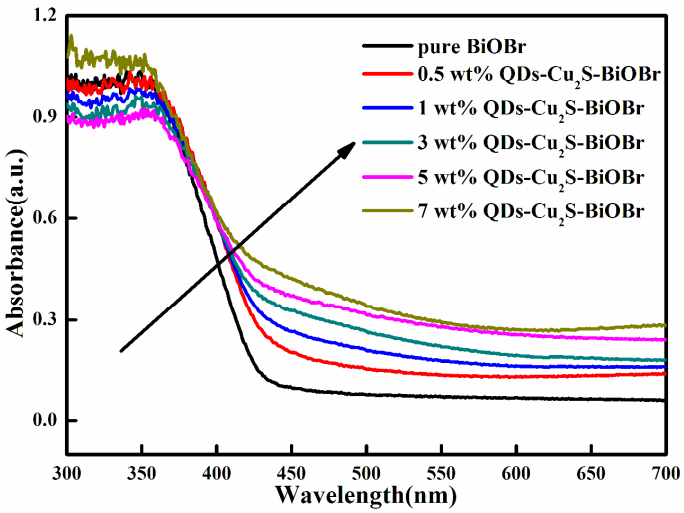

Fig. 6

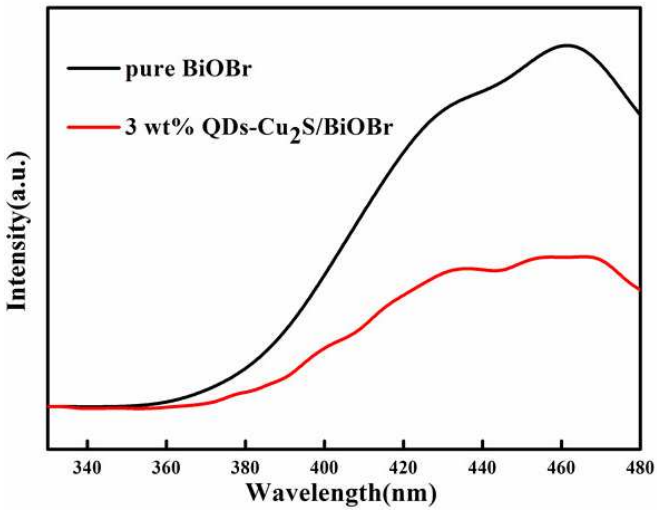

Fig. 7

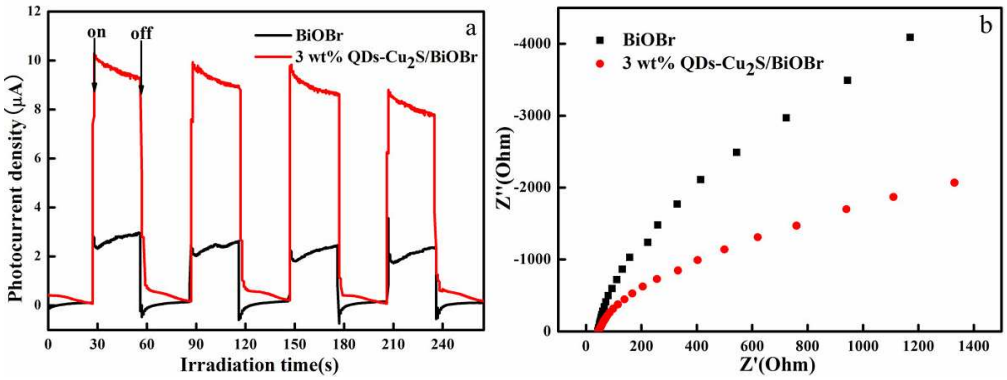

Fig. 8

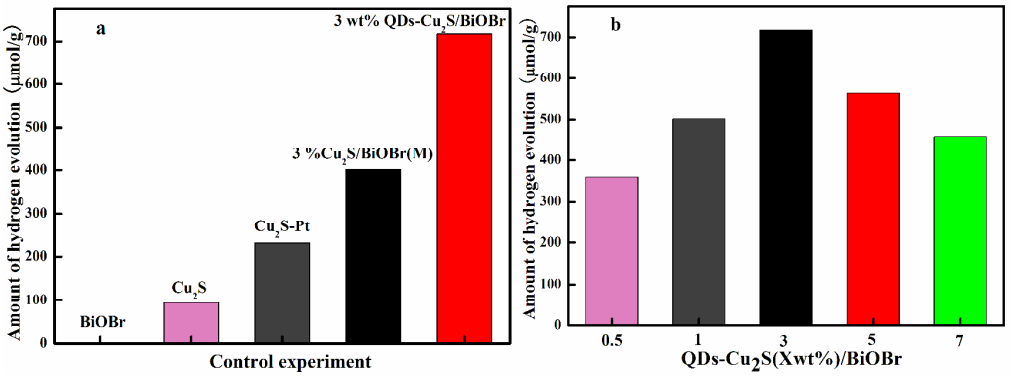

Fig. 9

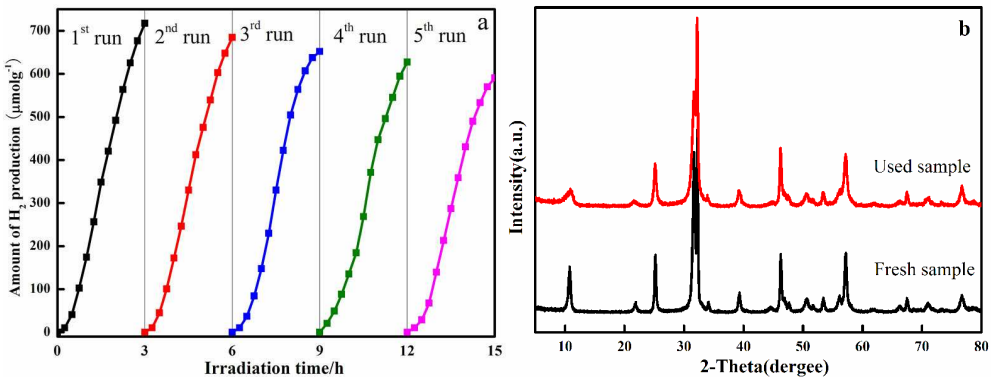

Fig. 10